The Clinicopathological Characteristics, MRI Features, And Radiation Dose Of Radio-Induced Brain Necrosis In Nasopharyngeal Carcinoma Patients

Minggu Zhong
Jiangmen Central Hospital
Yinglin Peng
Sun Yat-sen University Cancer Center
Siyue Mao
Sun Yat-sen University Cancer Center
YuKun Chen
Sun Yat-sen University
Hao Duan
Sun Yat-sen University Cancer Center
Suwen Wu
Sun Yat-sen University Cancer Center
Yi Wu
Jiangmen Central Hospital
Jiyong Gu
Jiangmen Central Hospital
Zhibin Li
Jiangmen Central Hospital
Enming Cui
Jiangmen Central Hospital
Jun Wen
Jiangmen Central Hospital
Shulan Liu
Jiangmen Central Hospital
YuJie Liu
Jiangmen Central Hospital
Ronglue Wei
Jiangmen Central Hospital
Junying Liu
Jiangmen Central Hospital

Zhongqin Luan
Jiangmen Central Hospital
Zize Feng
Jiangmen Central Hospital
Yilong Peng
Jiangmen Central Hospital
Wenguang Zhang
Jiangmen Central Hospital
Jiajun Dong
Jiangmen Central Hospital
Jun Dong (dongjun1@sysucc.org.cn)
Sun Yat-sen University Cancer Center

Research Article

Keywords: Radio-induced brain necrosis, nasopharyngeal carcinoma, radiotherapy

Posted Date: March 11th, 2022

DOI: https://doi.org/10.21203/rs.3.rs-1428133/v1

Abstract

Background: Radio-induced brain necrosis is a late-onset radiotherapy complication, especially in nasopharyngeal carcinoma (NPC) patients. We presented the clinicopathological characteristics, dynamic changes of MRI features, and radiation dose in the areas of radio-induced brain necrosis, which will shed light on preventing this severe radiotherapy complication.

Methods: We retrospectively collecting and reanalyzing clinical, imaging, radiation plans and pathological data from 48 NPC patients diagnosed with radio-induced brain necrosis and underwent craniotomy. To calculate the radiation dose in the areas of radio-induced brain necrosis, we reviewed the radiation plan of each patient and delineated the volume of the radio-induced brain necrosis. We also mapped the dynamic changes of magnetic resonance imaging (MRI) features and performed CD3, CD31, CD68, CD11b, Ki67, terminal deoxynucleotidyl transferase-dUTP nick end labeling (TUNEL) and HE staining on radio-induced brain necrosis specimens to observe pathological changes.

Results: The mean latency period for radio-induced brain necrosis was 9.23 years. According to the radiotherapy plans, the mean radiation dose for NPC was 7041±553 cGy. The mean dose to the radio-induced brain necrosis area was 5684.57±409.99 cGy. The necrotic areas exhibited high-intensity signals on T2-weighted images (WIs) and low-intensity signals on T1WIs over time. HE staining showed that the necrotic areas contained irregular fibers and inflammatory cells. The immunohistochemical results showed CD3(+), CD31(+), CD68(+), CD11b(+), Ki67(+), and TUNEL(+) cells in radio-induced brain necrosis specimens.

Conclusions: NPC patients who underwent radiotherapy and survived more than 5 years with hyperintense signals in temporal lobes in the T2WI should be paid close attention to radio-induced brain necrosis. A radiation dose no more than 5684.57±409.99 cGy in temporal lobes of NPC patients is recommended.

Background

Nasopharyngeal carcinoma (NPC) is an uncommon carcinoma worldwide, and 86500 cases of NPC, accounting for only 0.6% of all cancers, were reported in 2012(1). However, it is a prevalent carcinoma in China, especially in six southern provinces. In Guangzhou city, the agestandardized incidence rate (ASR) was 22.2 per 100 000 for males and 9.9 per 100 000 for females in 2002(2). Intensity-modulated radiotherapy (IMRT) is an ideal radiation modality for NPC(3) due to its favorable balance between target coverage and safety to adjacent organs(4).

As the survival for NPC patients has been greatly prolonged, IMRT may also lead to late complications, such as radio-induced brain necrosis(5, 6). The incidence of radio-induced brain necrosis in the setting of focal radiotherapy has been estimated as 3–24%(6, 7). Radiation may induce fibrinoid changes in the blood vessels and demyelination, which eventually leads to late neurological sequelae with or without

gross brain necrosis(8, 9). More importantly, the temporary or permanent adverse effects of radiation on the central nervous system will severely worsen the prognosis and quality of life of NPC patients.

With the help of magnetic resonance imaging (MRI) and computed tomography (CT), radio-induced brain necrosis is able to be diagnosed early(10). Although there are several practicable treatments, such as surgical resection, corticosteroids, hyperbaric oxygen therapy (HBOT), or bevacizumab, for radio-induced brain necrosis, the neurological sequelae of patients are largely irreversible(11).

Therefore, preventing radio-induced brain necrosis has been an important mission for clinicians. By collecting and reanalyzing clinical, imaging, radiation plans and pathological data from NPC patients who suffered from radio-induced brain necrosis, we presented the clinicopathological characteristics, dynamic changes of MRI features, and radiation dose in the areas of radio-induced brain necrosis, which will shed light on preventing this severe radiotherapy complication.

Patients And Methods

Clinical data

We retrospectively reviewed the clinical data of 48 NPC patients who were diagnosed with radio-induced brain necrosis at Jiangmen Central Hospital and Sun Yat-sen University Cancer Center between January 2008 and December 2016. All of these patients underwent craniotomy for their radio-induced brain necrosis because conservative treatments were confirmed unsuccessful with obviously neurological symptoms. The clinicopathological characteristics, including age at craniotomy, sex, pathological classification of NPC, tumor stage at initial diagnosis (according to 8th American Joint Committee on Cancer (AJCC) classification), radiation dosage, as well as latency period, initial symptoms, imaging features, pathologic findings, outcomes of radio-induced brain necrosis after radiotherapy, were collected.

This study was approved by the ethics committee of Sun Yat-sen University Cancer Center. Written informed consent was obtained from all the included patients. The dateset supporting the conclusions of this article is available in the public Research Data Deposit (RDD) platform (www.researchdata.org.cn) with approval (RDD Number RDDA2017000203).

Mri Data Collection

We retrospectively reviewed all the MRI data of the 48 NPC patients. The images were obtained on a head and neck MRI scanner from diagnosis of radio-induced brain necrosis to the end of follow-up after brain necrosis resection. We exported all the images and chose T1-weighted images (WIs), T2WIs, contrast-enhanced T1WIs, and diffusion-weighted images (DWIs) of every patient’s brain and nasopharynx region. We clearly mapped the dynamic changes in the features of radio-induced brain necrosis.

Radiation Dose Calculation

The radiation plans of 11 patients were obtained and reanalyzed successfully. The planning target volume (PTV) that was contoured in the radiotherapy program included the gross target volume of the nasopharynx (GTVnx), clinical target volume (CTV1), and clinical target of preventive radiation (CTV2). After delineation of the above target areas, the corresponding planning target areas (PTVnx, PTV1, and PTV2) were generated by expansion using the treatment planning system (TPS) (Eclipse Version 15.5, Varian, Palo Alto, California, USA) with setup errors. The organs at risk (OARs) that were contoured included the brain stem, spinal cord, lens, optic nerve, optic chiasm, pituitary gland, parotid gland, temporal lobe, temporomandibular joint (TMJ), and mandible. Nine dynamic intensity-modulated radiotherapy (dIMRT) synchronous doseplans were created using the TPS. The prescription dose and OAR dose constraints were applied to the treatment plans, with 6 MV X-ray radiationas the prescription doses for PTVnx, PTV1, and PTV2. The calculation grid of the planned dose was 3 mm × 3 mm × 3 mm. We delineated the areas of radio-induced brain necrosis according to the MRI images and summed the dose per unit volume (Fig. 1).

Immunohistochemistry (Ihc) And Terminal Deoxynucleotidyl Transferase-dutp Nick End Labeling (Tunel) Assay

Formalin-fixed, paraffin-embedded radio-induced brain necrosis specimens were sectioned at 5 μm. After being baked at 65°C for 1 hours, the samples were deparaffinized in xylene and rehydrated in a series of graded ethanol. For antigen retrieval, the sections were microwaved for 30 minutes in a repair solution (pH 9.0). Then, the samples were incubated with 3% hydrogen peroxide for 10 minutes to block endogenous peroxidase activity. The sections were incubated with the primary antibodies CD3 (1:200, ZA-0503-1.5, ZSGB-BIO, Beijing, China), CD31 (1:200, ZM-0044-1.5, ZSGB-BIO, Beijing, China), CD68 (1:200, ZM-0060-1.5, ZSGB-BIO, Beijing, China), CD11b (SAB, #46806, 1:150 dilution) and Ki-67 (1:200, ZM-0167-1.5, ZSGB-BIO, Beijing, China) in a 37°C incubator for 50 min. Subsequently, the samples were incubated with secondary antibodies and ABC reagent (#PK-7200, VECTOR LABORATORIES, Burlingame, CA, USA) at room temperature for 30 minutes. Immunoperoxidase staining was performed using an ImmPACT DAB Peroxidase Substrate (#SK-4105, VECTOR LABORATORIES, Burlingame, CA, USA) according to the manufacturer's recommendations. Apoptotic cells were identified using the Click-iT™ TUNEL Colorimetric IHC Detection Kit (C10625, Life Technologies, Carlsbad, CA, USA) following the manufacturer's instruction.

Statistical analysis

Descriptive statistics were used to analyze the clinical records and radiation doses, and the data are presented as the mean ± standard error (SE). The analyses were performed using the Statistical Package for the Social Science (SPSS version 16.0; SPSS Inc., Chicago, IL, USA).

Result

Patients' clinical characteristics

The clinicopathological characteristics of patients were summarized in Table 1. Thirty-six of the 48 patients were male. Median age at diagnosis of radio-induced brain necrosis was 50 years (range, 35–69 years). There were 9 patients with TNM stage II, 16 patients with stage III, and 23 patients with stage IVa NPC. The pathological subtypes included poorly differentiated squamous cell carcinoma (n = 23), Undifferentiated nonkeratinizing squamous cell carcinoma (UD-NKCs) (n = 22), and papillary adenocarcinoma (n = 3). Brain necrosis mostly developed in bilateral temporal lobe (n = 21), followed by left temporal lobe (n = 15) and right temporal lobe (n = 12). The range of latency period for the appearance of radio-induced brain necrosis was from 2.5 to 17.4 years, and the mean latency period was 9.2 years.

Table 1
Clinicopathological features of the patients with radiation-induced brain necrosis

Features	Number	Percentage (%)
Median age (range, years**)**	50 (35–69)	
Sex		
Male	36	75.0
Female	12	25.0
TNM stage		
II	9	18.8
III	16	33.3
IVa	23	47.9
Pathological type		
Poorly differentiated squamous cell carcinoma	23	47.9
Undifferentiated nonkeratinizing squamous cell carcinoma	22	45.8
Papillary adenocarcinoma	3	6.3
Sites of radiation-induced brain necrosis		
Left temporal lobe	15	31.3
Right temporal lobe	12	25.0
Bilateral temporal lobe	21	43.8

Brain Mri Features

As previously mentioned, MRI is an important method to identify radio-induced brain necrosis as early as possible. All the patients underwent MRI scanning every three to six months after radiotherapy for NPC. From these follow-up images, we mapped the changing imaging features. Necrotic areas were seen at 36 months after radiation treatment and appeared mostly in the temporal lobe. Initially, they only appeared as small hyperintense signals that appeared cloud-like on the T2WIs. Over time, an increasingly hyperintense signal appeared, and the necrotic areas increased in size. On the T1WIs, the necrotic areas appeared as hypointense signals. On the last scan before brain surgery, the necrotic areas showed apparent cystic changes, and the signals were close to the signal of cerebrospinal fluid. Interestingly, we also observed that the cyst wall was enhanced on the contrast-enhanced T1WIs images of some patients (Fig. 2).

Radiation Dose Results

The mean dose for NPC was 7041 ± 553 cGy. To calculate the real radiation dose in radio-induced brain necrosis, we further reviewed the radiotherapy plans and 11 patients with integrated radiation data were finally analyzed. The areas of radio-induced brain necrosis were delineated according to MRI findings and the doses per unit volume were analyzed. The mean dose the areas of radio-induced brain necrosis received was determined to be 5684.57 ± 409.99 cGy (Table 2).

Table 2
The radiation dose of cerebral lesions

Case no.	Lesion volume(cc)	Minimal dose (cGy)	Maximal dose (cGy)	Mean dose(cGy)
1	3.102	2519.5	6777.3	4706.5
2	0.174	6286.6	6362.9	6325.0
3	3.618	5497.9	6523.5	6060.1
4	1.650	5645.2	5941.2	5777.9
5	1.359	5351.4	5828.6	5719.7
6	1.833	5340.2	5661.7	5522.1
7	8.496	5309.0	5517.1	5401.3
8	1.680	5729.3	5959.4	5846.0
9	1.011	5590.3	5724.6	5679.4
10	0.780	5757.5	5935.4	5853.1
11	2.928	5525.5	5771.8	5639.2
Mean dose(cGy)	2.42	5322.95	6000.32	5684.57 ± 409.99

Pathological Features Of Radio-induced Brain Necrosis

We observed a large area of necrotic tissue and a portion of the normal brain tissue. The pathological results revealed that the necrotic area consisted of central liquefaction, cavities, inflammatory cells, and nerve cell degeneration. The central area showed massive necrosis according to eosinophil staining. Hemorrhage was also seen at this magnification. When hemorrhage occurred, the cell nucleus could not always be seen. As a result, we discovered only abundant homogeneous reddish cellular debris that appeared amorphous. The portion of hemorrhagic tissue developed fibrosis and was surrounded by chronic inflammatory cells (histocytes and macrophages accounted for the majority of these cells). In addition, we observed hemosiderin under magnification, indicating that previous hemorrhaging had occurred. Some vessel lumina were obviously dilated. The nerve cells in this area showed degeneration and even coagulation necrosis at different levels. To observe clear molecular changes associated with the imaging changes, we also performed IHC on the brain specimens obtained from surgery. In this study, we found that all necrotic brain tissues were CD3(+), CD31(+), CD68(+), CD11b(+), Ki-67(+), and TUNEL(+) based on the IHC results (Fig. 3).

Discussion

According to the literature, the incidence of newly diagnosed NPC is 0.6%(1). Radiotherapy has greatly prolonged the survival time of patients with NPC. The occurrence of cystic brain necrosis was approximately one-tenth of that of cerebral radiation-induced injury(12). Radiation-induced necrosis greatly affects the survival and quality of life of NPC patients after radical radiotherapy. Therefore, identifying the clinicopathological characteristics, dynamic changes of MRI features, and radiation dose in the areas of radio-induced brain necrosis are critical for preventing radio-induced brain necrosis.

According to a previous study, the initial mean dose of radiotherapy for NPC that caused brain necrosis was 69.5 ± 1.2 Gy(13). However, that study did not calculate the real radiation dose in the areas of radio-induced brain necrosis. In the current study, the mean latency period for the appearance of radio-induced brain necrosis was 9.23 ± 3.98 years, and the mean radiation dose for NPC was 7041 ± 553 cGy. Both the latency period and radiation dose at the primary carcinoma site were similar to those in a previous study. The mean radiation dose in the areas of radio-induced brain necrosis was 5684.57 ± 409.99 cGy, which indicated that radiotherapists should consider a radiation dose no more than 5684.57 ± 409.99 cGy in temporal lobes of NPC patients.

From the MRI results, we observed that the MRI images showed almost no changes within less than half a year after the patients underwent radiotherapy, and the patients presented no apparent symptoms. Subsequently, the MRI images showed hyperintense signals in the temporal lobe in the T2WIs, and some patients reported mild discomfort, such as dizziness. When the necrotic area fully formed, patients eventually developed severe symptoms such as intense headaches, nausea and vomiting. In this study, we mapped the dynamic changes of MRI features of radio-induced brain necrosis, allowing the diagnosis of radiation-induced brain necrosis as soon as an image shows a small hyperintense signal in the T2WI.

According to the pathological data and IHC results, we found that some vessel lumina were obviously dilated and some endothelial cells exhibited necrosis. When hemorrhage occurred, abundant homogeneous reddish cellular debris appeared, and inflammatory cells infiltrated the area. The nerve cells showed degeneration and different degrees of coagulation necrosis. We hypothesize that radio-induced brain necrosis causes secondary damage to the nervous system by endothelial cell degeneration after radiation(14). This is because endothelial cells undergo active mitosis more often than nerve cells, so they may be more sensitive to radiation. The autoimmune response may also be involved.

This study was limited by the retrospective features. Only 11 of the 48 patients were reanalyzed the radiation dose in the area of radio-induced brain necrosis. Future studies are warranted to confirm these preliminary results.

Conclusions

In summary, NPC patients who underwent radiotherapy and survived more than 5 years with hyperintense signals in temporal lobes in the T2WI should be paid close attention to radio-induced brain necrosis. A radiation dose no more than 5684.57 ± 409.99 cGy in temporal lobes of NPC patients is recommended.

Abbreviations

AST: Agestandardized incidence rate; AJCC: American Joint Committee on Cancer; CTV2: Clinical target of preventive radiation; CTV1: clinical target volume; CT: Computed tomography; DWIs: Diffusion-weighted images; dIMRT: Dynamic intensity-modulated radiotherapy; GTVnx: Gross target volume of the nasopharynx; HBOT: Hyperbaric oxygen therapy; IHC: Immunohistochemistry; IMRT: Intensity-modulated radiotherapy; MRI: Magnetic resonance imaging; NPC: Nasopharyngeal carcinoma; OARs: Organs at risk; PTV: Planning target volume; RDD: Research Data Deposit; SE: Standard error; TMJ: Temporomandibular joint; TUNEL: Terminal deoxynucleotidyl transferase-dUTP nick end labeling; TPS: Treatment planning system; UD-NKCs: Undifferentiated nonkeratinizing squamous cell carcinoma; WIs: Weighted images

Declarations

Ethics approval and consent to participate

This study was approved by the ethics committee of Sun Yat-sen University Cancer Center.

Consent for publication

Written informed consent was obtained from each patient.

Availability of data and materials

The dateset supporting the conclusions of this article is available in the public Research Data Deposit platform (www.researchdata.org.cn) with approval (RDD Number RDDA2017000203).

Competing interests

The authors declare that they have no competing interests

Funding

This project was supported by the National Science Foundation for Distinguished Young Scholars of China (Grant No. 81601581 and 81600606), the GuangDong Basic and Applied Basic Research Foundation (2020A1515110069) and the Science and Technology Program of Jiangmen, China (2018630100110019805).

Authors' contributions

(I) Conception and design: M.Z., Jiajun D., and Jun D.; (II) Literature search: M.Z., Y.P., S.M., H.D., Y.C.;(III) Administrative support: Y.W.; (IV) Provision of study materials or patients: K.S., X.Z., J.G., Z.L., E.C., J.W., S.L., Y.L., R.W., J.L., Z.L., Z.F., Y.P., and W.Z.; (V) Collection and assembly of data: M.Z. X.Y., S.W., and Z.W.; (VI) Image analysis: M.Z., Y.P., and S.M.; (VII) Data analysis and interpretation: M.Z., Y.P., and S.M.; (VIII) Manuscript writing: M.Z., Y.P., S.M., H.D., Jiajun D., and Jun.D.; (IX) Final approval of manuscript: All authors.

Acknowledgments

We thank patients and their families for their participation and contribution to the project.

References

1. Chua MLK, Wee JTS, Hui EP, Chan ATC. Nasopharyngeal carcinoma. Lancet. 2016;387(10022):1012–24.
2. Wee JT, Ha TC, Loong SL, Qian CN. Is nasopharyngeal cancer really a "Cantonese cancer"? Chin J Cancer. 2010;29(5):517–26.
3. Network NCC. (NCCN)Clinical Practice Guidelines in Oncology 2019 [Version 1:[
4. Lv JW, Huang XD, Chen YP, Zhou GQ, Tang LL, Mao YP, et al. A National Study of Survival Trends and Conditional Survival in Nasopharyngeal Carcinoma: Analysis of the National Population-Based Surveillance Epidemiology and End Results Registry. Cancer Res Treat. 2018;50(2):324–34.
5. Miyatake S, Nonoguchi N, Furuse M, Yoritsune E, Miyata T, Kawabata S, et al. Pathophysiology, Diagnosis, and Treatment of Radiation Necrosis in the Brain. Neurol Med Chir (Tokyo). 2015;55 Suppl 1:50–9.
6. Kong F, Zhou J, Du C, He X, Kong L, Hu C, et al. Long-term survival and late complications of intensity-modulated radiotherapy for recurrent nasopharyngeal carcinoma. BMC Cancer. 2018;18(1):1139.
7. Marks JE, Baglan RJ, Prassad SC, Blank WF. Cerebral radionecrosis: incidence and risk in relation to dose, time, fractionation and volume. Int J Radiat Oncol Biol Phys. 1981;7(2):243–52.
8. Chong VF, Fan YF, Chan LL. Temporal lobe necrosis in nasopharyngeal carcinoma: pictorial essay. Australas Radiol. 1997;41(4):392–7.
9. Sundgren PC, Cao Y. Brain irradiation: effects on normal brain parenchyma and radiation injury. Neuroimaging Clin N Am. 2009;19(4):657–68.
10. Chao ST, Ahluwalia MS, Barnett GH, Stevens GH, Murphy ES, Stockham AL, et al. Challenges with the diagnosis and treatment of cerebral radiation necrosis. Int J Radiat Oncol Biol Phys. 2013;87(3):449–57.
11. Drezner N, Hardy KK, Wells E, Vezina G, Ho CY, Packer RJ, et al. Treatment of pediatric cerebral radiation necrosis: a systematic review. J Neurooncol. 2016;130(1):141–8.
12. Marks JE, Wong J. The risk of cerebral radionecrosis in relation to dose, time and fractionation. A follow-up study. Prog Exp Tumor Res. 1985;29:210–8.
13. Fang W, Gu B, Jing X, Xiao S, Fan S, Liao W, et al. Late-onset cystic brain necrosis after radiotherapy for nasopharyngeal carcinoma. Jpn J Clin Oncol. 2017;47(6):499–504.
14. Lohmann P, Stoffels G, Ceccon G, Rapp M, Sabel M, Filss CP, et al. Radiation injury vs. recurrent brain metastasis: combining textural feature radiomics analysis and standard parameters may increase (18)F-FET PET accuracy without dynamic scans. Eur Radiol. 2017;27(7):2916–27.

Figures

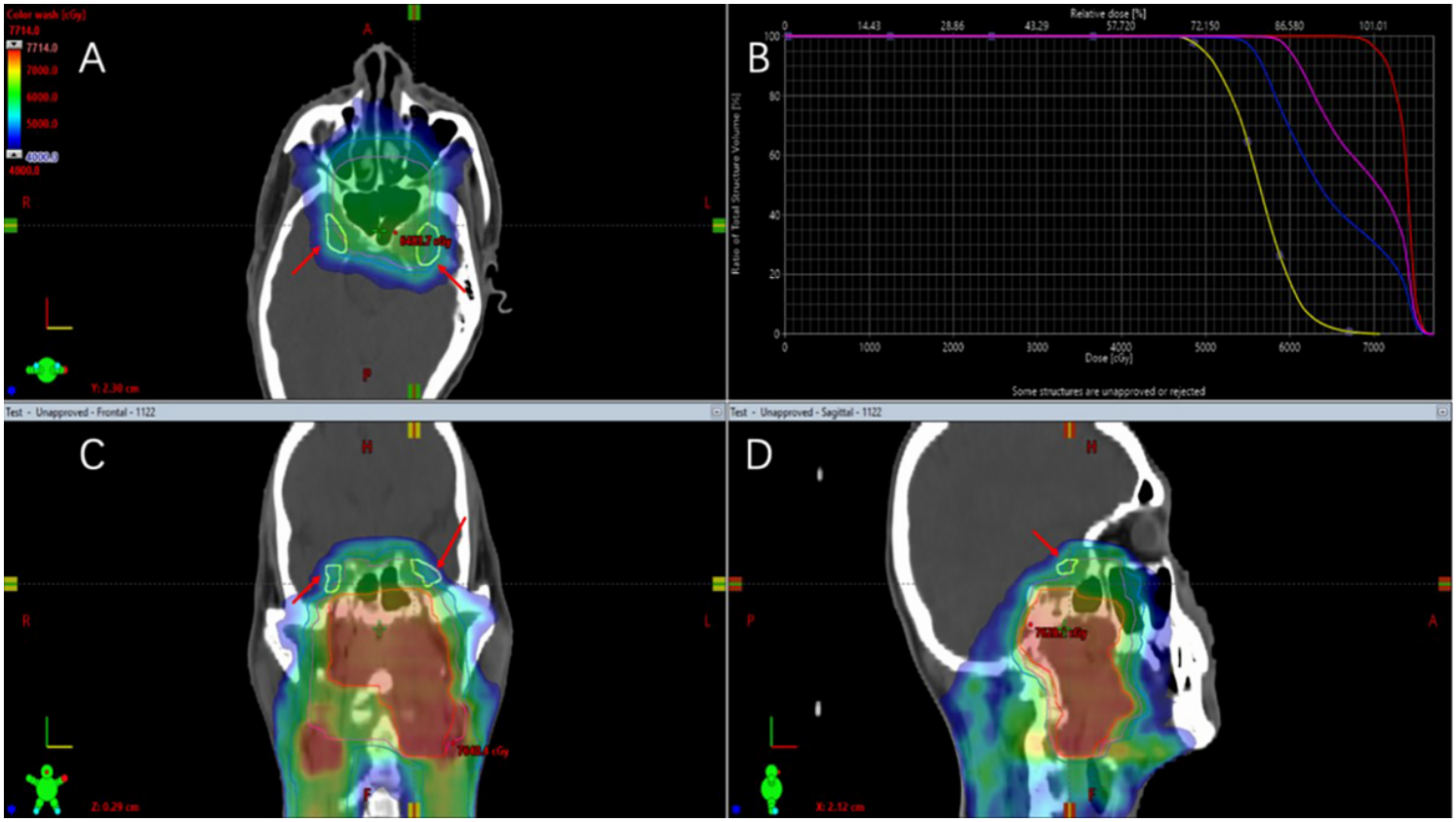

Figure 1

Calculation of the irradiation dosage in brain radiation injury lesions. A, C and D are the dose distribution diagrams of patients in the cross-sectional, coronal and sagittal planes, respectively. In the diagrams, the red is planning target volume of the nasopharynx (PTVnx), the pink is PTV1, and the blue is PTV2. The yellow area is the area of temporal lobe injury (arrow notes the position). B shows the dose-volume histogram (DVH) of PTVnx, PTV1, PTV2 and the injury regions.

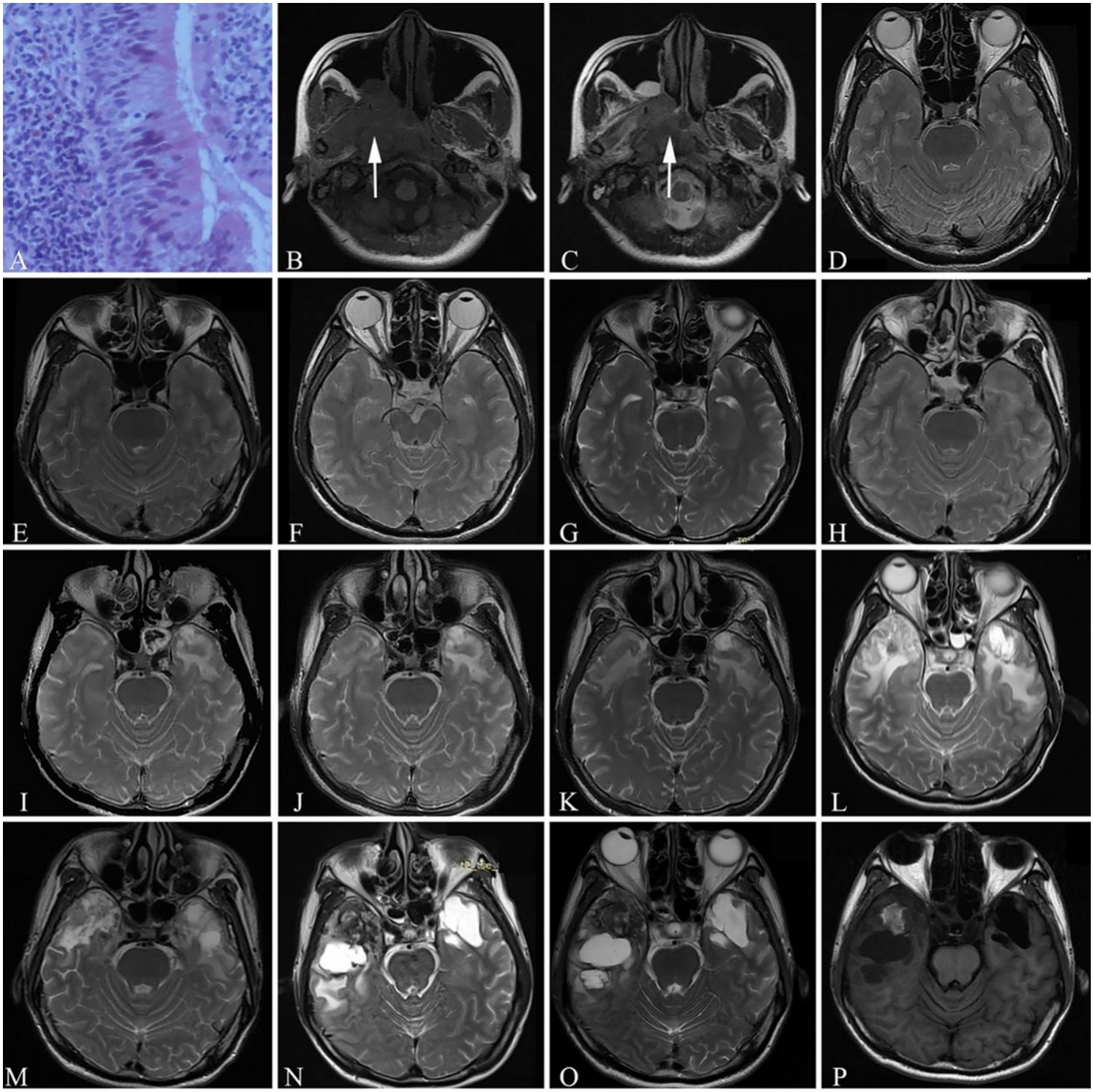

Figure 2

Dynamic changes in brain radiation injury on MRI. A is the histopathological examination result of a patient's nasopharynx tissue. B is the T1WI, and C is the T2WI of the nasopharynx. The back wall of the nasopharynx is incrassated (White arrow). D is the T2WI of the normal cerebrum before radiotherapy. E to N are the T2WIs at several reexaminations after radiotherapy. From E to G are images from one month after radiotherapy to one year after radiotherapy. There is nothing changed in the cerebrum. H is an image at 3 years after radiotherapy. From H to N, the images seem to indicate changes of brain necrosis. N is an

image at 7 years after radiotherapy; the lesion becomes increasingly apparent, and the signal is increasingly intense on T2WIs. O and P images are T2 and T1WIs before surgery. The necrotic brain tissue shows cystic degeneration.

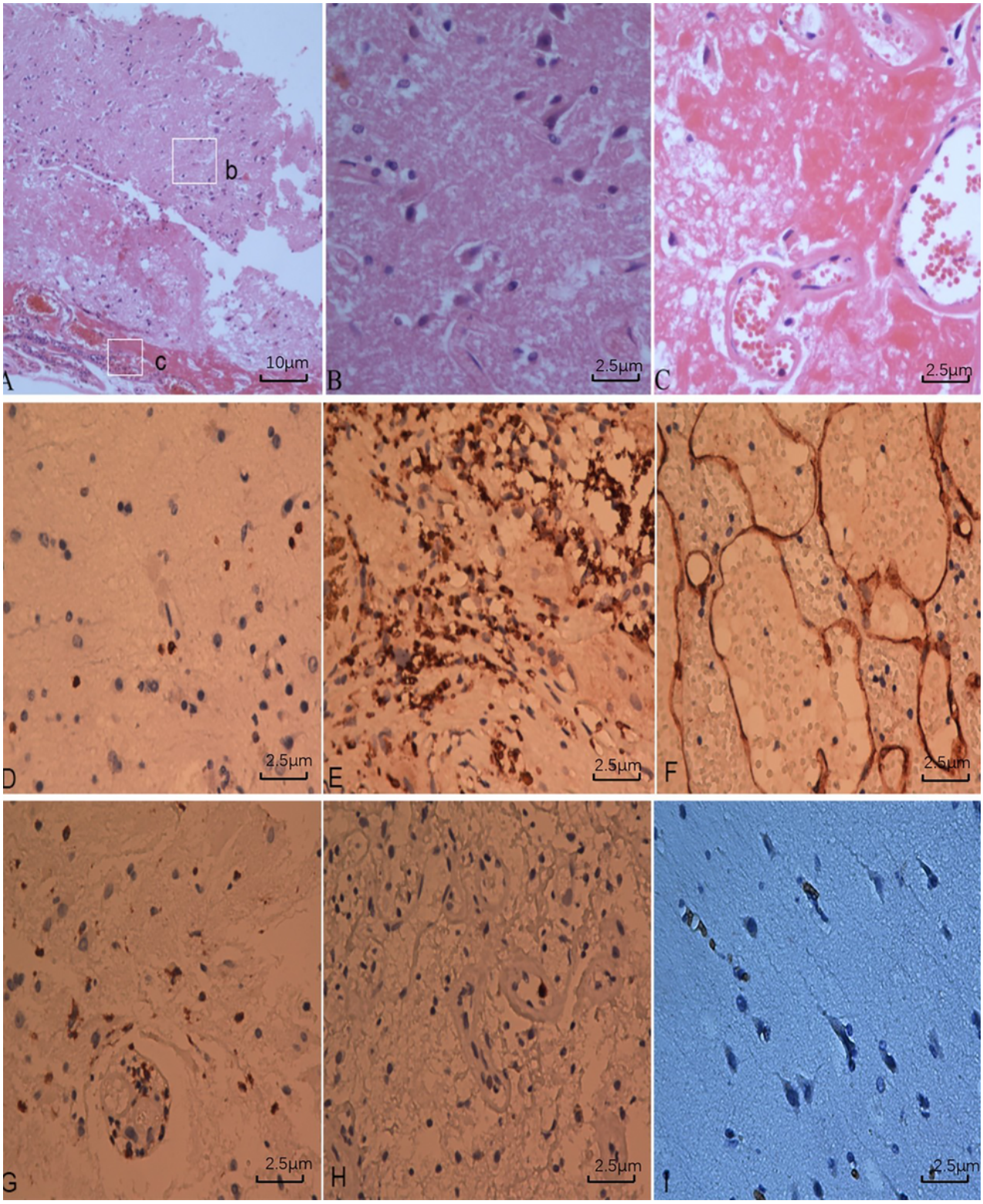

Figure 3

H&E and immunohistochemistry results of the brain necrosis specimens. A shows a large area of necrotic tissue. White frame (b) is the area of necrotic tissue. White frame (c) is the area of hemorrhaging between the necrotic and normal tissue. B is the amplification of white frame (b). C is the amplification of white frame (c). D shows the CD3 staining positive result. E shows the CD31 staining result. F shows the CD68 staining result. G shows the CD116 staining result. H shows the Ki-67 staining result. I show the TUNEL staining result.